

Copyright © 1981, by the author(s).
All rights reserved.

Permission to make digital or hard copies of all or part of this work for personal or classroom use is granted without fee provided that copies are not made or distributed for profit or commercial advantage and that copies bear this notice and the full citation on the first page. To copy otherwise, to republish, to post on servers or to redistribute to lists, requires prior specific permission.

QUASINEUTRAL HYBRID SIMULATION OF
MACROSCOPIC PLASMA

by

Douglas S. Harned

Memorandum No. UCB/ERL M81/71

14 September 1981

ELECTRONICS RESEARCH LABORATORY
College of Engineering
University of California, Berkeley
94720

Quasineutral Hybrid Simulation of Macroscopic Plasma

Phenomena

Douglas S. Harned

Electronics Research Laboratory

University of California

Berkeley, CA 94720

ABSTRACT

A method for solving the quasineutral hybrid plasma equations in two dimensions is presented, using full ion dynamics and inertialess electrons. The method is extended to allow plasma-vacuum interfaces of arbitrary shape. The algorithm is applied to the study of rotational instabilities in theta pinch Vlasov equilibria.

I. INTRODUCTION

Many macroscopic problems in plasma physics are characterized by ion Larmor radii comparable to the scale lengths of the system. For these problems, and for problems involving microinstabilities, a fluid description of the ions is inadequate, and the ions must instead be treated in a fully kinetic manner. Also, as plasma behavior dominated by ion physics generally evolves on time scales much longer than characteristic electron time scales, for many problems it is unnecessary to follow the full dynamics of the electron motion. In addition, when the frequencies of interest are low compared to the ion cyclotron frequency, $\omega < \omega_{ci}$, the effects of high frequency phenomena, such as electromagnetic radiation and electron inertia, are generally negligible. These considerations have led to the development of quasineutral hybrid plasma simulation codes. Such one-dimensional hybrid simulations have been performed by Sgro and Nielson¹ for theta pinch implosions and by Byers et al.² for the study of microinstabilities. Two-dimensional (r-z) simulations of theta pinch implosions have been performed by Hewett³.

Our hybrid algorithm treats ions as particles and electrons as an inertialess fluid. The Darwin version of Maxwell's equations (i.e., neglecting the transverse displacement current) is used. The electron momentum equation, with inertial terms neglected, is coupled with Maxwell's equations and the statement of quasineutrality in order to determine the electric and magnetic fields. Section II of this paper describes our two-dimensional quasineutral model which has been applied to ion layer kink instabilities. Section III discusses the extension of this algorithm to problems having plasma-vacuum interfaces. In Sec. IV we show the application of the method to the study of theta pinch rotational instabilities.

II. MODEL

This section describes the quasineutral model and the basic algorithm used in simulation. Ampere's law may be decomposed into its longitudinal (curl-free) and transverse (divergence-free) parts:

$$\nabla \times \bar{B} = \frac{4\pi \bar{J}_t}{c} + \frac{1}{c} \frac{\partial \bar{E}_t}{\partial t} \quad (1a)$$

$$0 = \frac{4\pi \bar{J}_l}{c} + \frac{1}{c} \frac{\partial \bar{E}_l}{\partial t} \quad (1b)$$

where the subscripts l and t , respectively, refer to the longitudinal and transverse parts of a vector quantity. We assume quasineutrality, setting $n_i = n_e$, which implies that $\nabla \cdot \bar{J} = 0$. If \bar{J}_l vanishes at the boundaries, or if the system has periodic boundaries, then $\bar{J}_l = 0$ throughout the system. For the study of low frequency phenomena, the Darwin approximation is made, that is, the transverse displacement current is neglected. Ampere's law then reduces to the simple form

$$\nabla \times \bar{B} = \frac{4\pi}{c} (\bar{J}_e + \bar{J}_i) \quad (2)$$

where \bar{J}_e and \bar{J}_i refer to the electron and ion current densities.

Electrons are treated as a fluid so that their motion is assumed to be described by the electron momentum equation

$$n_e m_e \frac{d\bar{v}_e}{dt} = -en_e (\bar{E} + \bar{v}_e \times \bar{B}/c) - \nabla P_e \quad (3)$$

where m_e is the electron mass, n_e the electron density, \bar{v}_e the electron drift velocity, and P_e the scalar electron pressure. For low frequency modes electron inertia effects are not important. Therefore, the left hand side of Eq. 3 is set equal to zero. With the electron current expressed as $\bar{J}_e = -en\bar{v}_e$ and the assumption of quasineutrality, Eqs. 2 and 3 may be combined to produce an expression for the electric field

$$\bar{E} = \frac{1}{4\pi n_i e} (\nabla \times \bar{B}) \times \bar{B} - \frac{1}{n_i e c} \bar{J}_i \times \bar{B} - \frac{1}{n_i e} \nabla (n_i T_e) \quad (4)$$

where T_e is the electron temperature. Equation 4 determines the electric field as a function of the magnetic field, electron temperature, ion current, and ion density. Ion currents and densities are determined by linear weighting (particle-in-cell). The magnetic field is advanced by Faraday's law

$$\partial \bar{B} / \partial t = -c \nabla \times \bar{E} \quad (5)$$

and the ion particle positions and velocities are determined by integrating the equations of motion

$$\bar{d}v / dt = \frac{q}{m_i} (\bar{E} + \bar{v} \times \bar{B} / c). \quad (6a)$$

$$\bar{d}x / dt = \bar{v} \quad (6b)$$

A two-dimensional simulation code has been developed using this model. The equations are solved in cartesian coordinates with no variation in the z-direction (i.e., $\partial/\partial z=0$). The magnetic field is $\bar{B}=B_z \hat{z}$ and the quantities J_z , E_z , and v_z are all set equal to zero. Particle motion is followed by a standard leap-frog integrator. The time advance of field quantities given by Eqs. 4 and 5 is accomplished by a predictor-corrector algorithm. This algorithm, as follows, is similar in form to one used in one-dimensional computations by Byers et al². If the quantities $\bar{J}_i^{n+\frac{1}{2}}$, $\bar{v}_i^{n+\frac{1}{2}}$, $n_i^{n+\frac{1}{2}}$, \bar{B}^n , and \bar{E}^n are known, the magnetic field is advanced by

$$\bar{B}^{n+\frac{1}{2}} = \bar{B}^n - (c\Delta t/2) \nabla \times \bar{E}^n. \quad (7a)$$

A prediction is then made for \bar{E}^{n+1} and \bar{B}^{n+1} by

$$\bar{E}_{pred}^{n+1} = -\bar{E}^n + 2\bar{E}(\bar{J}_i, n_i, \bar{B}, P_e)^{n+\frac{1}{2}} \quad (7b)$$

$$\bar{B}_{pred}^{n+1} = \bar{B}^{n+\frac{1}{2}} - (c\Delta t/2) \nabla \times \bar{E}_{pred}^{n+1} \quad (7c)$$

Using the predicted fields, a predictor particle move is performed to obtain $n_i^{n+\frac{3}{2}}$ and $\bar{J}_{i,pred}^{n+\frac{3}{2}}$ after which $\bar{B}_{pred}^{n+\frac{3}{2}}$ is predicted by

$$\bar{B}_{pred}^{n+\frac{3}{2}} = \bar{B}_{pred}^{n+1} - (c\Delta t/2) \nabla \times \bar{E}_{pred}^{n+1}. \quad (7d)$$

Finally, the new electric and magnetic fields are obtained from

$$\bar{E}^{n+1} = \frac{1}{2} \bar{E}(\bar{J}_i, n_i, \bar{B}, P_e)^{n+\frac{1}{2}} + \frac{1}{2} \bar{E}(\bar{J}_i, n_i, \bar{B}, P_e)_{pred}^{n+\frac{3}{2}} \quad (7e)$$

$$\bar{B}^{n+1} = \bar{B}^{n+\frac{1}{2}} - (c\Delta t/2) \nabla \times \bar{E}^{n+1}. \quad (7f)$$

The particle positions can now be advanced to $n+\frac{3}{2}$ using these new field quantities.

The electric and magnetic fields are stored on interlaced grids. Spatial derivatives are determined by four-point operators, e.g.,

$$(\partial E_x / \partial x)_{i+\frac{1}{2}, j+\frac{1}{2}} = [(E_x)_{i+1, j+1} + (E_x)_{i+1, j} - (E_x)_{i, j+1} - (E_x)_{i, j}] / 2\Delta x \quad (8)$$

This algorithm is second order accurate in time and space. The time step is limited by a Courant-Friedrichs-Lewy (CFL) condition on the Alfvén speed, $\Delta t < (\Delta x / v_A)$, where $v_A \equiv B_0 c / (4\pi n_i m_i)^{1/2}$. An additional constraint on the time step for stability is $\omega_{ci} \Delta t < 2$; however, in practice the CFL condition is the more restrictive requirement. The algorithm of Eqs. 7 has been successfully applied in a code using doubly periodic boundaries to study kink instabilities in field-reversed ion layers; these results are discussed elsewhere⁴.

III. PLASMA-VACUUM INTERFACES

The preceding algorithm has the disadvantage that it cannot treat properly low density or vacuum regions, where $n_i \rightarrow 0$. We desire to avoid the details of sheath regions or describing low density plasma regions with high accuracy, since the

quasineutral hybrid model is not well suited for such problems. However, we would like to include the gross effects due to the fields extending into vacuum regions, such as wall stabilization. Additionally, in highly nonlinear problems, density fluctuations may occur which cause low density or vacuum ($n_i \rightarrow 0$) regions to arise in a small number of isolated cells. These will cause local violations of the CFL condition which are sufficient to terminate the simulation unless an alternate method can be found for determining the field quantities in these cells. One possible solution is the addition of a low density plasma throughout the vacuum region which maintains sufficient plasma density so that the CFL condition is satisfied. However, this method does not produce the instantaneous signal propagation that should occur across a vacuum. Additionally, for a highly nonlinear problem, large amplitude waves are likely to occur in the low density region which can still cause the CFL condition to be violated.

It is desirable to use a method to treat vacuum regions that does not involve the monitoring of complicated, moving, plasma-vacuum interfaces. One such method is described by Hewett³, where the resistivity is varied in moving from the plasma to the vacuum regions in a nonlinear ADI solution. We have developed another way to include vacuum regions by modification of Eqs. 7b and 7e in the algorithm of Sec. II. Two constants, c_p and c_v , are defined so that in the vacuum $c_p=0$ and $c_v=1$ while in the plasma $c_p=1$ and $c_v=0$. Then Eq. 7b is replaced by

$$c_p \bar{E}_{pred}^{n+1} + c_v \nabla^2 \bar{E}_{pred}^{n+1} = c_p (-\bar{E}^n + 2\bar{E}(\bar{J}_i, n_i, \bar{B}, P_e)^{n+\frac{1}{2}}) \quad (9a)$$

and Eq. 7e is replaced by

$$c_p \bar{E}^{n+1} + c_v \nabla^2 \bar{E}^{n+1} = c_p \left(\frac{1}{2} \bar{E}(\bar{J}_i, n_i, \bar{B}, P_e)^{n+\frac{1}{2}} + \frac{1}{2} \bar{E}(\bar{J}_i, n_i, \bar{B}, P_e)^{n+\frac{3}{2}} \right) \quad (9b)$$

A grid point is defined to be plasma if $n_i \geq n_c$ and vacuum if $n_i < n_c$, where n_c is a

cutoff density, as illustrated in Fig. 1. The effect of the modification is that Eqs. 9a and 9b solve the plasma equations, Eqs. 7b and 7e, in the plasma and then solve $\nabla^2 \bar{E}=0$, the vacuum electric field solution, in the vacuum. The magnetic field is still advanced by Eqs. 7a, 7c, 7d, and 7f. These equations provide values for B_z in the plasma, in the vacuum, and at the conducting wall. The vacuum field is then smoothed by solving $\nabla^2 B_z=0$ in the vacuum with the known values of B_z in the plasma and along the conducting wall as boundary conditions. The left hand side of Eq. 9 is constantly changing as the plasma moves; however, it is solved easily by an iterative matrix solver. Note that no monitoring of the plasma-vacuum interface is required. The Courant-Friedrichs-Lewy condition is now imposed on the Alfvén speed at the density cutoff, n_c . For the magnetic field, this algorithm effectively solves $\nabla^2 \bar{A}=0$ in the vacuum. This method adequately treats fluctuations in low density plasma regions and is capable of handling highly dynamical problems, as well. However, for the study of slowly evolving plasma behavior, such as theta pinch rotational instabilities with growth rates much less than the ion cyclotron frequency, additional care must be taken, as follows.

In our two-dimensional model the theta pinch equilibrium is a cylindrical plasma with an azimuthal current density $\bar{J}=J_\theta(r)\hat{\theta}$. The initial plasma density is finite at radii $r < r_p$. A vacuum region extends from $r=r_p$ to a conducting wall at $r=r_w$. An axisymmetric theta pinch equilibrium must satisfy the radial force balance equation

$$0 = -\frac{B_z}{4\pi} \frac{\partial B_z}{\partial r} - \frac{\partial P}{\partial r} + n_i m_i r \Omega_i^2, \quad (10)$$

where Ω_i is the mean ion rotational frequency. Near r_p , the first term on the right hand side of Eq. 10, the magnetic force term, represents the inward force due to magnetic pressure. The other two terms, the thermal pressure term and the centrifugal

force term, are both outward near r_p . An equilibrium may easily be set up which obeys Eq. 10 over the bulk of the plasma. However, near the plasma-vacuum interface the algorithm of Eqs. 7 and 9 produces diffusion. The reason for this diffusion is that in a region with plasma density below the cutoff density, n_c , the magnetic field is constant, because this region is considered to be vacuum and $\nabla^2 \bar{A} = 0$ is effectively solved there (rather than $\nabla^2 \bar{A} = 4\pi \bar{J}/c$). Since the current is set to zero where $n_c > n_i > 0$, the magnetic force term in this region is also zero. Consequently, the plasma near the interface will diffuse radially because it only sees the outward forces due to the plasma pressure and the centrifugal force of the rotating ions. The error here corresponds to the neglect of the small amount of current density (both ion and electron) carried by the low density plasma, which in the laboratory provides the $\bar{J} \times \bar{B}$ force that contains the plasma at its edge.

An alternate method for treating plasma-vacuum interfaces has been devised for our two-dimensional simulation code. The plasma is now considered to be in three regions, rather than two. The regions are shown schematically in Fig. 2. The plasma region is still defined to be that with density above n_c . The vacuum region is defined to be that with zero density or $n_i < n_v$, where n_v is a cutoff value smaller than n_c . The transition region is the region with $n_v < n_i < n_c$. The electric field is solved as described by Eq. 9. The magnetic field in the plasma region is determined by the plasma equations, Eqs. 7. However, to maintain the current below the cutoff, n_c , a different vacuum solution is used. For the vacuum region the plasma is assumed to be a perfect conductor, hence, vacuum magnetic flux is assumed to be conserved. For this two-dimensional problem the magnetic field at a given time will be uniform throughout the vacuum. Therefore, B_z^{vac} may be determined by

$$B_z^{vac}(t) = \int_{vac} B_z^{vac}(t=0) \cdot dA / A_{vac}(t) \quad (11)$$

where A_{vac} is the area of the vacuum region. Once the vacuum and plasma solutions are known, the two solutions are connected by solving $\nabla^2 B_z = 0$ in the transition region with Dirichlet boundary conditions given by the magnetic fields determined in the vacuum and plasma regions. The effect of this solution on the equilibrium is that the magnetic field now corresponds to that which would be present if the missing current below the cutoff existed in the transition region. If $\partial/\partial\theta=0$, this current in the transition region is distributed so that the transition azimuthal current density is proportional to $1/r$, since $\nabla^2 B_z = 0$ is solved in that region. The transition region is typically only one or two grid cells in thickness; however, maintaining a finite $\partial B_z/\partial r$ there is critical, as our results demonstrate. Sometimes small internal vacuum regions may occur due to fluctuations which arise in the nonlinear stage of a rotational instability. It is possible to search for such small regions and to handle them as transition cells by solving $\nabla^2 B_z = 0$. The method does not yet appear to be easily applicable to complicated plasma-vacuum interfaces in which large internal vacuum regions exist.

IV. APPLICATION TO THETA PINCH ROTATIONAL INSTABILITIES

We have studied rotating theta pinches starting from exponential rigid rotor Vlasov equilibria⁵. With Ω_e defined as the mean rotational frequency of the electrons, the current density as a function of radius is described by

$$J_\theta(r) = -en_0(\Omega_e - \Omega_i) \operatorname{sech}^2 \left(\frac{r^2 \pm r_1^2}{r_0^2} \right) \quad (12)$$

and the corresponding magnetic field profile is

$$B_z(r) = \frac{cm_i \Omega_i^2}{e(\Omega_e - \Omega_i)} + \frac{c(T_e + T_i)}{e(\Omega_e - \Omega_i) r_0^2} \tanh \left(\frac{r^2 \pm r_1^2}{r_0^2} \right). \quad (13)$$

The sign preceding r_1^2 in Eqs. 12 and 13 is positive for non-reversed equilibria (i.e., when $B_z(0) > 0$). For $\Omega_i = 0$ or r_1 sufficiently large, a negative sign preceding r_1^2 corresponds to a field-reversed equilibrium (i.e., $B_z(0) < 0$). A parameter, α , is defined such that $\alpha = -\Omega_i / (\Omega_e - \Omega_i)$. The case $\alpha = 0$ corresponds to a stationary thermal (Maxwellian) ion distribution, with all of the current carried by the electrons. This configuration should be stable, according to finite Larmor radius fluid theory⁶ and Vlasov-fluid theory⁷. We now demonstrate the difference between the two-region and three-region solutions. Simulations have been performed with a density cutoff, n_c , at three per cent of the peak density. The spatial grid is a 100 by 100 mesh. 50,000 particles are used to represent the ions and the time step is $\omega_{ci} \Delta t = 0.1$. Figure 3 shows the evolution of the radial density profile (averaged over θ) with time for the two-region solution. The plasma diffusion at the edge eventually leads to the diffusion of the bulk of the plasma, demonstrating that with the two-region solution it is impossible to maintain an equilibrium for times long compared to the ion-cyclotron period. In contrast, the result for the three-region solution is shown in Fig. 4. The diffusion at the edge has been virtually eliminated and the equilibrium density profile is maintained. It was found possible to reduce the plasma expansion in the two-region solution by using a lower cutoff density; however, since the time step is limited by the CFL condition on the cutoff density, unacceptably small time steps, from an economics standpoint, were required to eliminate the expansion effectively. It may be possible to use a more implicit method, for which the time step is not restricted by the CFL condition at the cutoff density, in order to improve the results of the two-region solution.

We have done simulations starting from non-reversed rigid rotor theta pinch equilibria with $\alpha > 0$. These simulations have $(\Omega_e - \Omega_i) / \omega_{ci} = 0.022$ and $\beta_0 = 0.75$. β_0 is

the "beta-on-axis", $\beta_0 = n_i(0) T / (B_0^2 / 8\pi)$, where $n_i(0)$ is the initial density at $r=0$ and B_0 is the magnitude of the external magnetic field. No instabilities have been observed for non-reversed equilibria with $\alpha=1.0$. However, for $\alpha=2.0$ an $m=2$ instability, where m is the azimuthal mode number, is evident. These observations are in agreement with the theoretical predictions of Freidberg and Pearlstein⁶ and Seyler⁷. Figure 5 shows the initial ion particle positions for an equilibrium with $\alpha=2.0$. Seyler⁷ predicts the growth rate for this equilibrium to be $(\gamma/\omega_{ci})=0.025$ and the real frequency to be $(\omega_r/\omega_{ci})=0.033$. The two-region solution is not feasible for this problem because the plasma expansion would obscure the instability on these time scales. Therefore, the three-region method is used. In our simulation, at $t=144\omega_{ci}^{-1}$, an $m=2$ instability, where m is the azimuthal mode number, has grown to large amplitude as can be seen from the ion particle positions shown in Fig. 6.

The quantity $\delta r(t, \theta) \equiv \langle r \rangle - \langle r(t=0) \rangle$ is stored as a diagnostic and decomposed into its azimuthal Fourier components. In Fig. 7 is plotted $(\delta r)^2$ for mode 2, which gives an approximate measure of instability growth. The broken line in Fig. 7 corresponds to $(\delta r)^2$ for the growth rate of Seyler⁷ and shows that the growth we observe in our simulation is comparable. We have estimated the real part of the frequency, ω_r , by measuring the rotation of the elliptically deformed plasma cross-section. For this simulation run we find $(\omega_r/\omega_{ci})=0.035 \pm 0.005$. The value determined by Seyler⁷, $(\omega_r/\omega_{ci})=0.033$, is within the range of error of our simulation estimate.

Further details of the code are presented in Appendix A.1.

V. SUMMARY

A two-dimensional predictor-corrector method for quasineutral plasma simulation, similar to that used in one-dimensional computations by Byers et al.², has been developed. The method has been extended to allow the inclusion of vacuum and low density regions. A simple, two-region, treatment of the plasma-vacuum interface has been found inadequate for the study of instabilities with growth rates much smaller than the ion-cyclotron frequency. For such problems we have implemented a three-region method of solution which avoids the problems of diffusion at the interface found in the two-region method and avoids finding the details of the sheath. The simulation model has been successfully applied to the study of ion layer kink instabilities and theta pinch rotational instabilities.

ACKNOWLEDGMENTS

The author is indebted to Prof. C.K. Birdsall for his discussions, advice, and encouragement during the course of this work. Also acknowledged are the many valuable discussions held with Drs. D.W. Hewett, A. Friedman, and B.I. Cohen.

This work was supported by ONR Contract No. N00014-17-C0578. Computations were performed at the National Magnetic Fusion Energy Computer Center at Livermore.

REFERENCES

1. A.G. Sgro and C.W. Nielson, "Hybrid Studies of Ion Dynamics and Magnetic Field Diffusion During Pinch Implosions", *Phys. Fluids* **19**, pp. 126-133 (1976).
2. J.A. Byers, B.I. Cohen, W.C. Condit, and J.D. Hanson, "Hybrid Simulation of Quasineutral Phenomena in Magnetized Plasma", *J. Comput. Phys.* **27**, pp. 363-396 (1978).
3. D.W. Hewett, "A Global Method of Solving the Electron Field Equations in a Zero-Inertia-Electron-Hybrid Plasma Simulation Code", *J. Comput. Phys.* **38**, pp. 378-395 (1980)
4. D.S. Harned, "Kink Instabilities in Long Ion Layers", in preparation for submittal to *Phys. Fluids*.
5. R.L. Morse and J.P. Freidberg, "Rigid Drift Model of High-Temperature Plasma Containment", *Phys. Fluids* **13**, pp. 531-533 (1970).
6. J.P. Freidberg and L.D. Pearlstein, "Rotational Instabilities in a Theta Pinch", *Phys. Fluids* **21**, pp. 1207-1217 (1978).
7. C.E. Seyler, "Vlasov-Fluid Stability of a Rotating Theta Pinch", *Phys. Fluids* **22**, pp. 2324-2330 (1979).

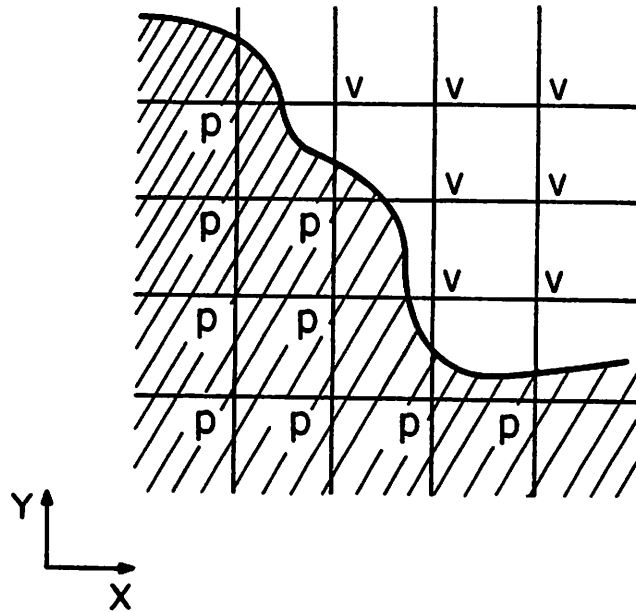


FIG. 1. A schematic of the grid used in the two-region solution. The shaded area corresponds to the plasma region, $n_i > n_c$ and the unshaded region to the vacuum, $n_i < n_c$. In order to calculate the field quantities at a given point, the operator to be applied is determined automatically by whether that grid point is in the vacuum (v) or in the plasma region (p).

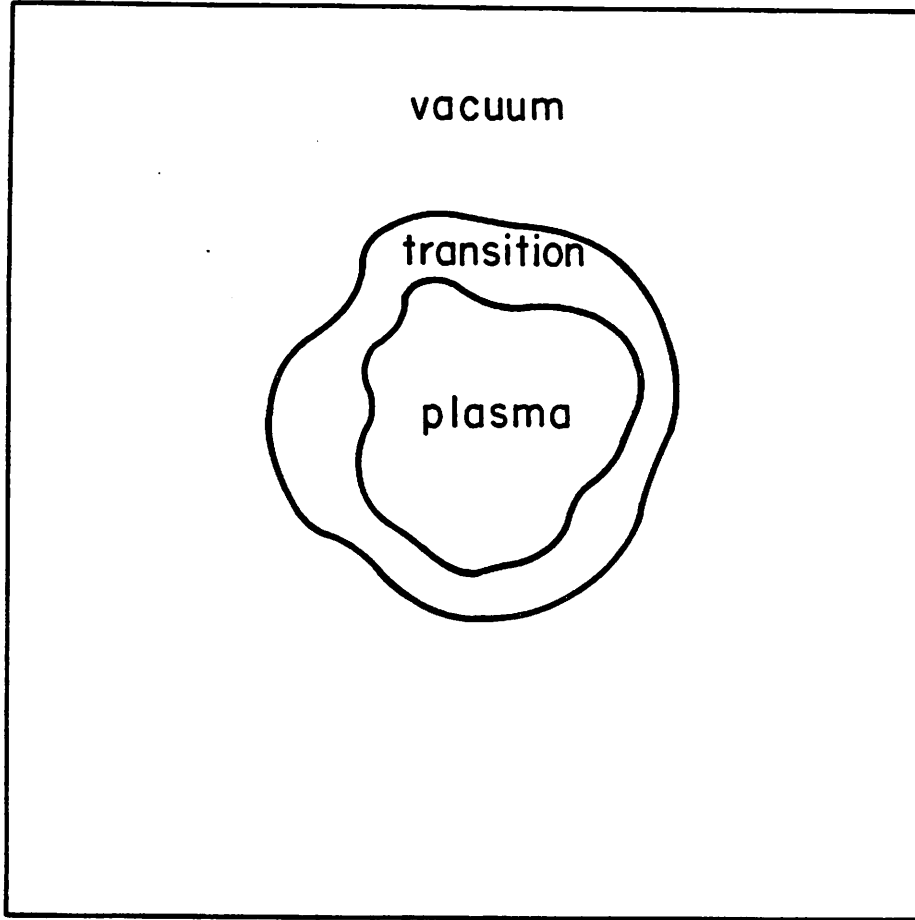


FIG. 2. The three regions for the plasma-vacuum system used in the theta pinch rotational instability problem.

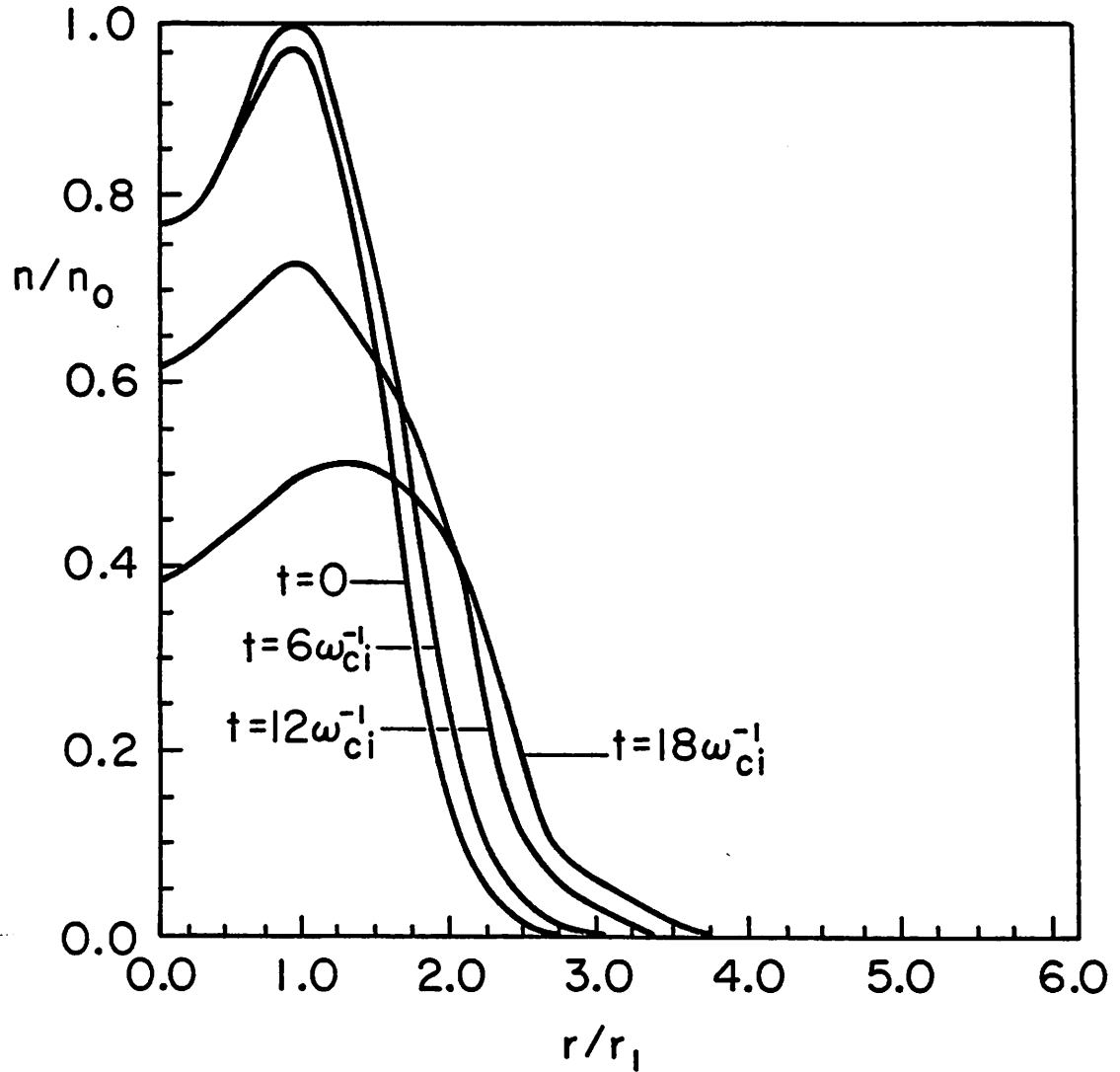


FIG. 3. Theta pinch density profiles, $n_i(r)$, at $t=0, 6, 12,$ and $18\omega_{ci}^{-1}$ for the two-region solution, showing the radial diffusion of the supposedly stable plasma due to the lack of current and the resulting $\vec{J} \times \vec{B}$ force at the plasma boundary, a numerical defect.

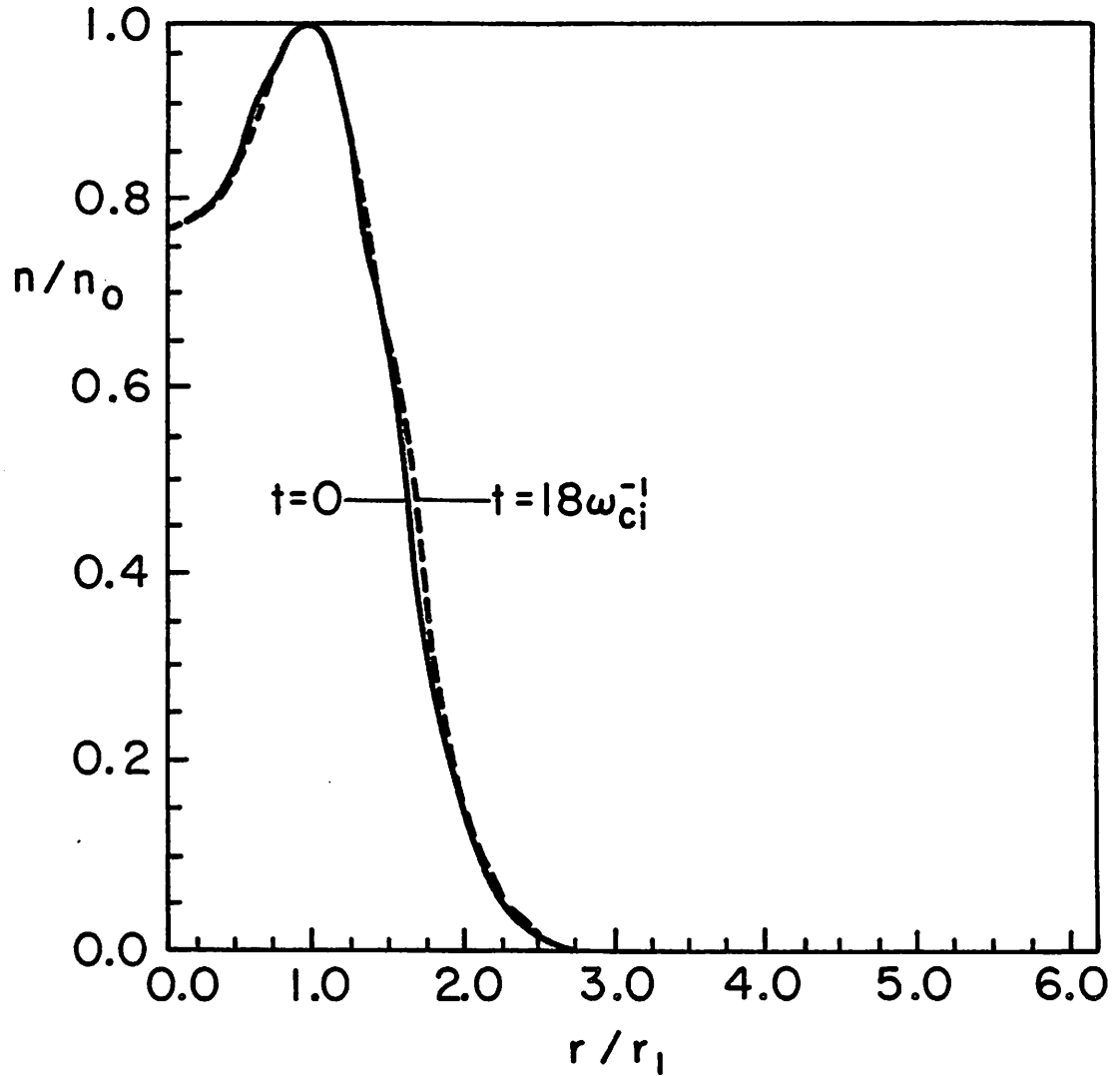


FIG. 4. Theta pinch density profiles, $n_i(r)$, at $t=0$ and $t=18\omega_{ci}^{-1}$ for the three-region solution. The diffusion present in the two-region solution has been eliminated and the density profile of the stable plasma is correctly maintained.

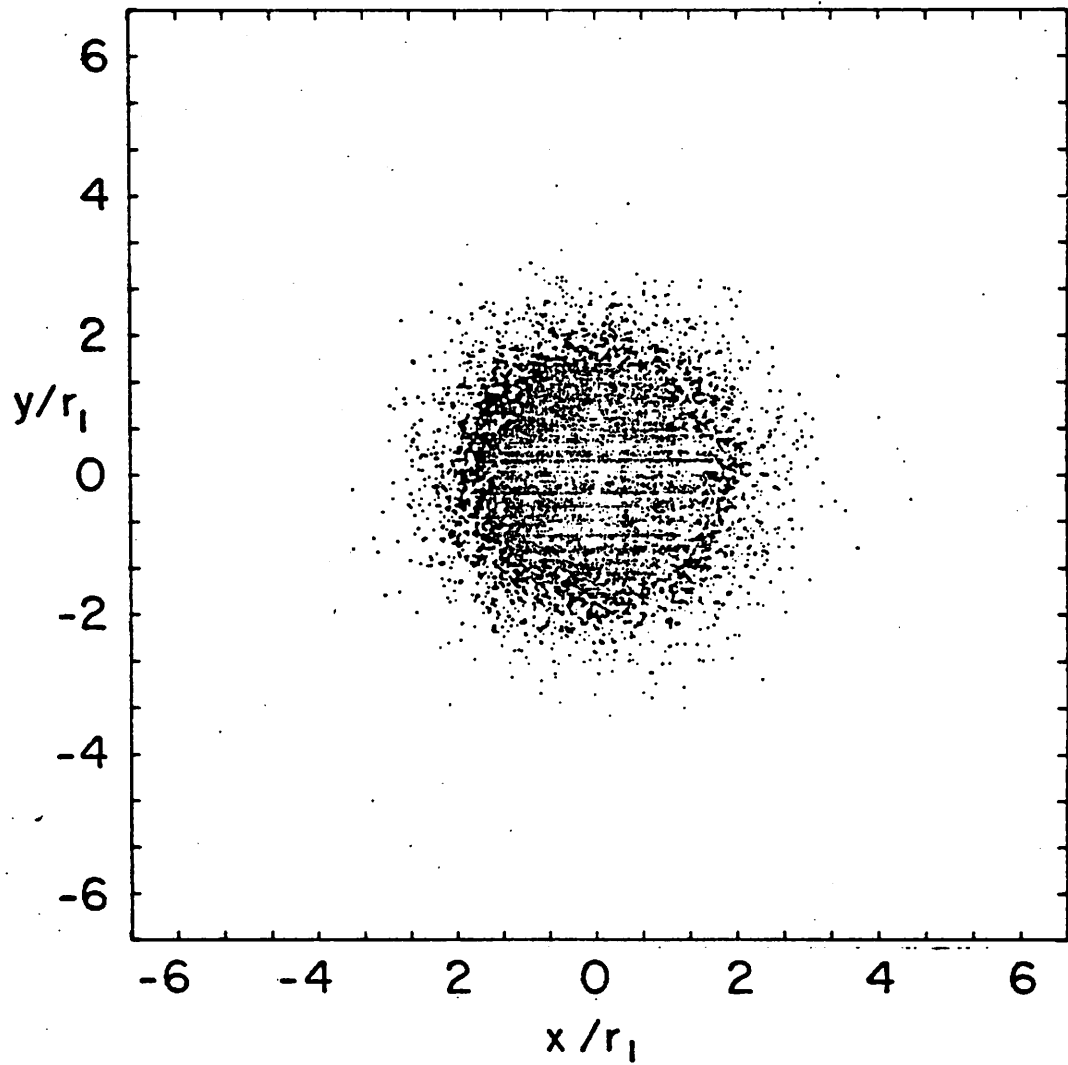


FIG. 5. Initial particle positions for a rigid rotor theta pinch equilibrium.

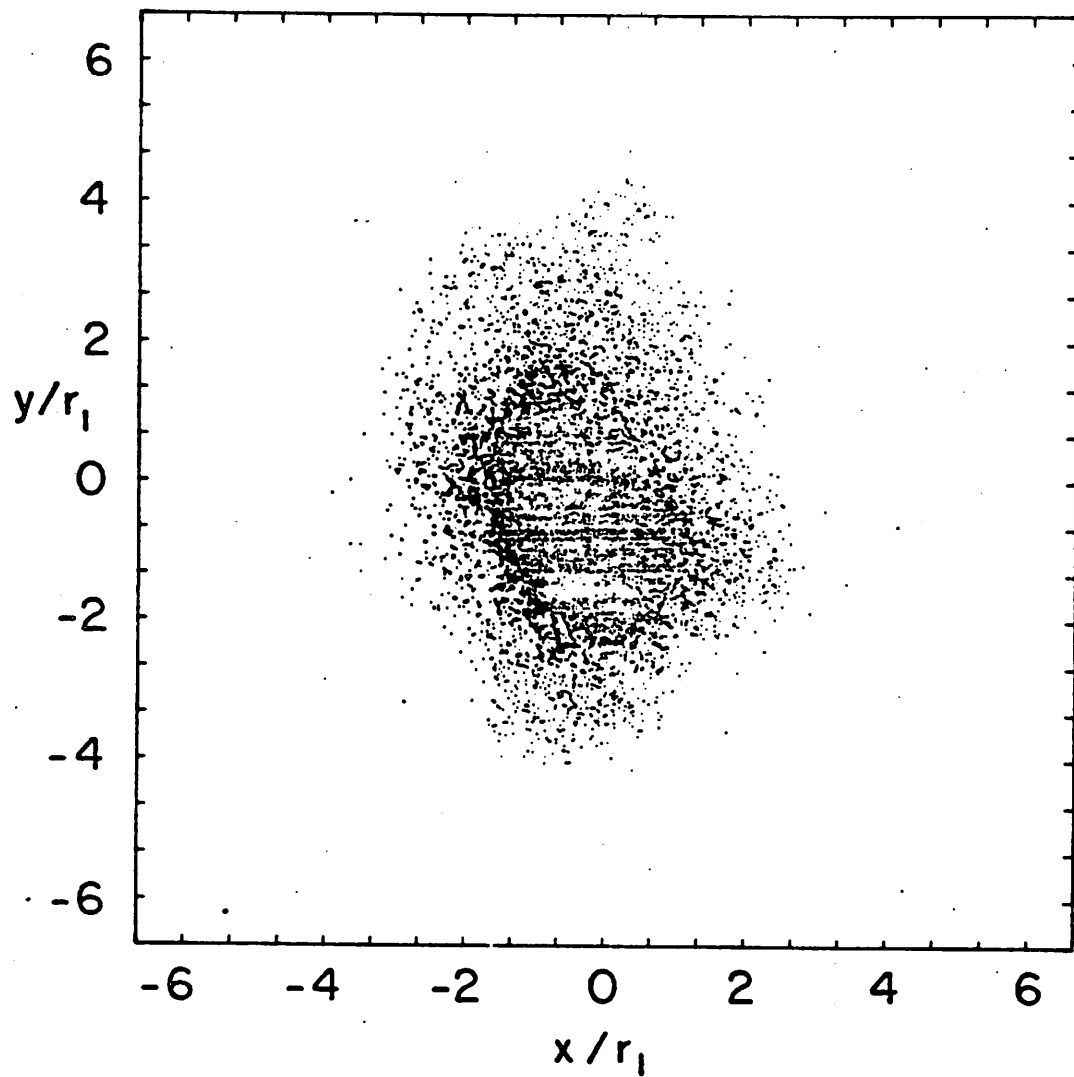


FIG. 6. Theta pinch particle positions at $t=144\omega_{ci}^{-1}$, after an $m=2$ instability has grown to large amplitude.

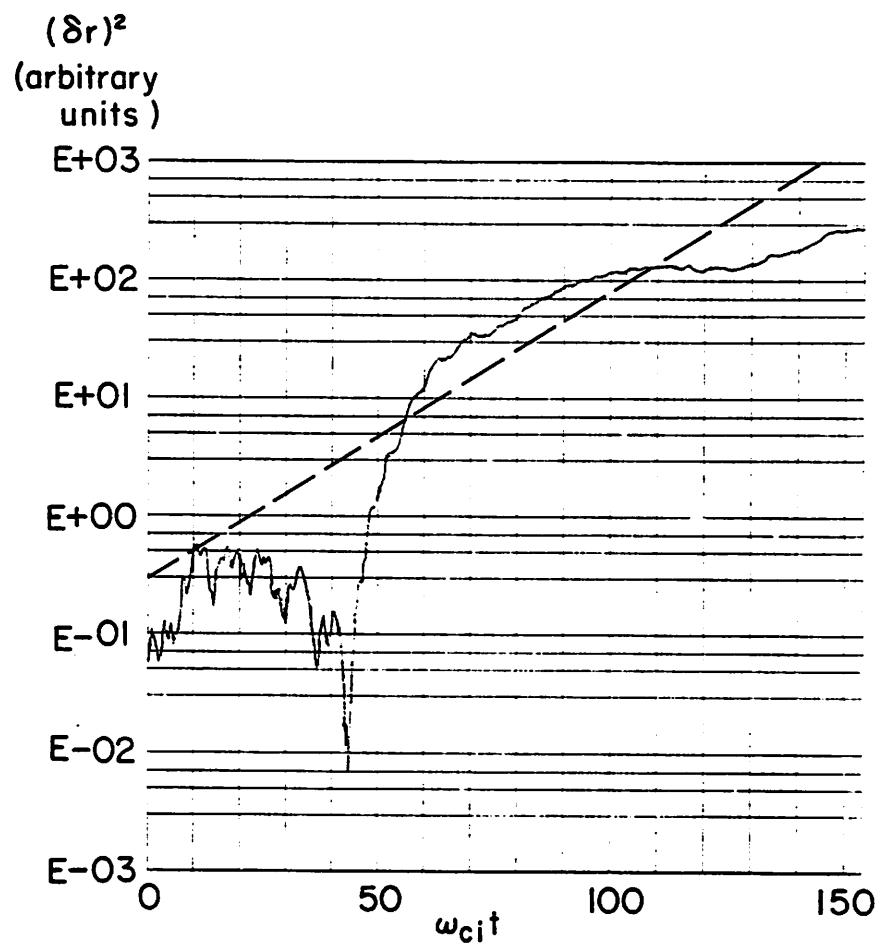


FIG. 7. $(\delta r(t))^2$ for the $m=2$ mode. The dashed line corresponds to the growth rate predicted by Seyler ($\gamma/\omega_{ci}=0.025$).

A.1 Description of Simulation Code

The algorithm used to advance the field quantities in our two-dimensional hybrid code, AQUARIUS, is similar to a one-dimensional method used by Byers et al.¹ Both methods have similar stability characteristics. The corrector iteration is necessary to prevent spurious odd-even oscillations from producing undesirable high frequency noise. The improvement with the corrector iteration can be seen in Figs. 1 and 2 which show the oscillation of Alfvén waves. Figure 1, the result without a corrector iteration, clearly shows the odd-even oscillation. This odd-even oscillation is not present in the predictor-corrector results of Fig. 2. These figures are taken from our results using a one-dimensional version of AQUARIUS. We have found convergence to be sufficient after one correction, so that further iterations are unnecessary.

Unlike the algorithms of Byers et al.¹, we use \bar{B} directly from Faraday's law rather than computing it from the vector potential, \bar{A} . This choice was made because in two dimensions, without axisymmetry, direct computation avoids the difficulty of decomposing the electric field into its longitudinal (curl-free) and transverse (divergence-free) parts for use in Faraday's law. We have chosen to calculate \bar{E} and \bar{B} on separate grids because it prevents the numerical diffusion and instabilities often associated with the computation of both quantities on the same grid. This choice is similar to the procedure used in other electromagnetic codes; e.g., Boris et al.². Our predictor-corrector method appears to be simpler than the two-dimensional nonlinear

ADI method of Hewett³. However, the more implicit nature of Hewett's method may allow a lower density cutoff for a given time step.

Our simulation model consists of four separate parts:

1. RREQUI is a program which loads particles into an exponential rigid rotor distribution in r , θ , v_r , and v_θ . The coordinates are then transformed to x , y , v_x , and v_y and written to a file, AQLOAD, as input to AQUARIUS.
2. AQUARIUS is the main program which solves the time dependent field and particle equations.
3. AQPPMD is a post-processor which reads as input a file produced by AQUARIUS. This input file contains the average radii of the plasma for 64 different angles at selected time intervals. The post-processor then performs a Fourier decomposition in θ to determine history information concerning individual modes. This history information is written in the form of a graphics file.
4. AQPPHST is a general post-processor for history information. This post-processor reads a history file from AQUARIUS which contains an assortment of information at selected time intervals, such as particle trajectories, kinetic energy, and field energies. This information is plotted and written to a graphics file.

AQUARIUS simulations begin by the reading of two input files:

1. INAQ provides approximately 50 basic parameters for the simulation, such as grid size, time step, and type and frequency of diagnostics.

2. **AQLOAD** provides the particle positions, as well as parameters to determine the magnetic field initialization for rigid rotor distributions as calculated by **RREQUI**.

After the input data has been read and the initial particle positions and magnetic field quantities determined, the electric field is initialized by the equation

$$\vec{E} = \frac{1}{4\pi ne}(\nabla \times \vec{B}) \times \vec{B} - \frac{1}{nec} \vec{J}_i \times \vec{B} - \frac{1}{ne} \nabla P_e$$

The initialization is finally completed by the subroutine **SETV** which performs a backward integration of the ion particle velocities by one half time step, so that the leap-frog mover will be properly centered with positions and velocities one half time step out of phase.

Once the initialization is complete, the main time loop begins. This loop is repeated until **IT**, the time step number, equals **NT**, the designated number of time steps for the run. Each time step begins with a particle move using the subroutine **MOVER**. **MOVER** performs a standard leap-frog advance of the particle positions and velocities. The subroutine **MOVER** also accumulates ion densities and ion current densities by linear weighting (particle-in-cell). A thorough discussion of particle-in-cell techniques and leap-frog particle movers can be found in Ref. 4. **MOVER** is vectorized for implementation on a Cray-1 computer. The vectorization has been found to produce a factor of 2.7 increase in speed over the same routine without vectorization. After the particle move is completed, the subroutine **FIELDS** is called. **FIELDS** performs the field advance described in the main section. It utilizes the subroutines **CALCE** and **BADV** to advance the electron and magnetic fields. When low density or vacuum regions are present, **CALCE** and **BADV** call subroutines to perform matrix solutions to Eqs. 9a and 9b. The matrix solutions use successive over-relaxation with

points ordered so that this method becomes fully vectorizable. An iterative scheme was chosen because:

1. As the plasma moves the vacuum regions change, changing the matrix structure each time step, so that a direct method would have to be fully repeated each time step.
2. A good guess is available from the previous time step.
3. High accuracy for the vacuum fields is not required.

Successive over-relaxation was chosen because it may be vectorized easily and because it requires no additional storage of temporary vectors.

After the field calculation has been completed in the time loop, diagnostic information is calculated. In the input data, different "snapshot" diagnostics may be requested at selected time intervals, such as:

1. Phase space plots.
2. Field, current, and density contour plots.
3. Field, current, and density cross-section plots.
4. $B_z(r)$, $E_r(r)$, $E_\theta(r)$, $J_{i,r}(r)$, $J_{i,\theta}(r)$, and $n_i(r)$ averaged over theta.
5. $B_z(\theta)$, $E_r(\theta)$, $E_\theta(\theta)$, $J_{i,r}(\theta)$, $J_{i,\theta}(\theta)$, and $n_i(\theta)$ for a selected radius.
6. Line printer contour plots.

Additionally, history information is written at selected intervals to serve as input for the post-processors AQPPMD and AQPPHST. After the last time step, $IT=NT$, the output files are closed and AQUARIUS ends. Because all history information is written into post-processor files, it is unnecessary to complete a given run in order to

access the information.

The dominant part of the time required to run AQUARIUS is used in MOVER. Each particle move takes approximately $8\mu s$ per time step of Cray-1 CPU time. When there are no vacuum regions, the time taken by the field solve is negligible. For a typical theta pinch run, with large vacuum regions, the field solve generally takes about 0.2 s for a 100 by 100 grid; this is about half of the time required to move 50,000 particles.

References

1. J.A. Byers, B.I. Cohen, W.C. Condit, and J.D. Hanson, "Hybrid Simulation of Quasineutral Phenomena in Magnetized Plasma", *J. Comput. Phys.* **27**, pp. 363-396 (1978).
2. J.P. Boris, "Relativistic Plasma Simulation - Optimization of a Hybrid Code", *Proceedings of the Fourth Conference on Numerical Simulation of Plasmas*, pp. 3-67 (NRL, Washington, 1970).
3. D.W. Hewett, "A Global Method of Solving the Electron-Field Equations in a Zero-Inertia-Electron-Hybrid Plasma Simulation Code", *J. Comput. Phys.* **38**, pp. 378-395 (1980).
4. C.K. Birdsall and A.B. Langdon, *Plasma Physics via Computer Simulation*, McGraw-Hill, in press.

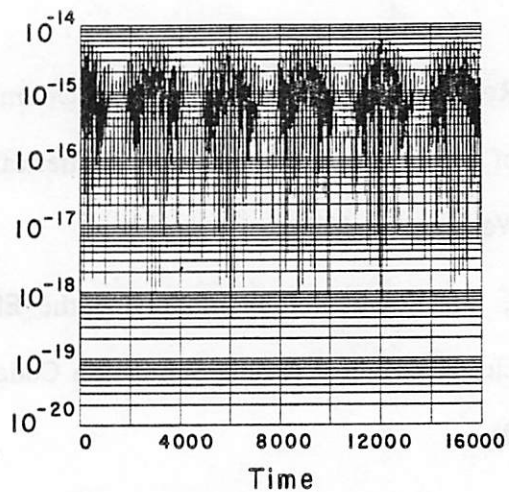


FIG. A1 Transverse electric field energy for Alfvén waves, showing the odd-even oscillations which exist without a corrector iteration (from a 1d simulation).

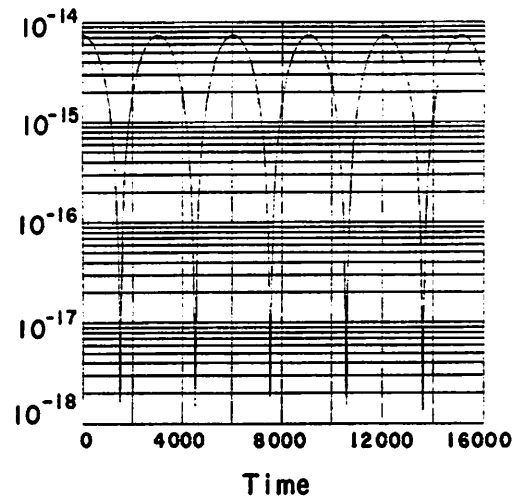


FIG.A2 Transverse electric field energy for Alfvén waves using the predictor-corrector method in a 1d simulation.